Research Article

Qingyang Fan*, Heng Liu, Li Jiang, Wei Zhang, Yanxing Song, Qun Wei*, Xinhai Yu, and Sining Yun*

Three-dimensional metallic carbon allotropes with superhardness

https://doi.org/10.1515/ntrev-2021-0079
received August 2, 2021; accepted September 1, 2021

Abstract: Three novel three-dimensional orthorhombic carbon phases are proposed based on first-principles calculations in this work. These phases possess dynamic stability and mechanical stability and are theoretically more favorable in energy compared to most other carbon allotropes. The hardness levels of *o*P-C_{16}, *o*P-C_{20}, and *o*P-C_{24} are 47.5, 49.6, and 55.3 GPa, respectively, which are greater than those of T10, T18, and O12 carbon. In addition, although *o*P-C_{16}, *o*P-C_{20}, and *o*P-C_{24} are metals, their ideal shear strengths are also greater than those of common metals such as Cu, Fe, and Al. Due to p_y electrons crossing the Fermi level, *o*P-C_{16}, *o*P-C_{20}, and *o*P-C_{24} show metallicity, and their charge densities of the band decomposition suggest that all the conductive directions of *o*P-C_{16}, *o*P-C_{20}, and *o*P-C_{24} are exhibited along the *a*- and *b*-axis, similar to C_5.

Keywords: metallic carbon, superhard material, electronic properties, conductive directions

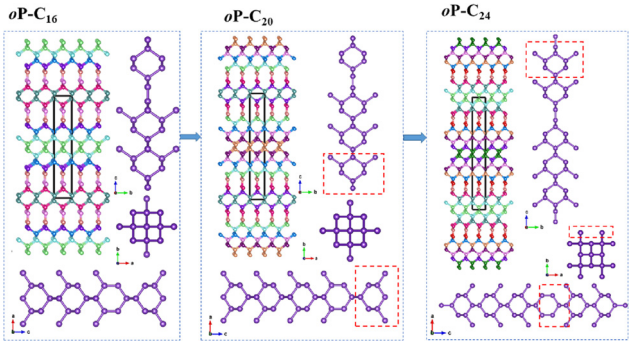

Graphical abstract: The crystal structures of *o*P-C_{16}, *o*P-C_{20}, and *o*P-C_{24}.

1 Introduction

The rapid growth of computer performance and the abundance of various experimental data have led to the intensified exploration of new energy materials [1] and novel electronic information materials. The use of computers for scientific calculations is already the third scientific method for mankind to understand and conquer nature after theoretical science and experimental science. Due to the extensive role and important influence of metal superhard carbon materials in the fields of industry, machinery, and aerospace, there is an urgent need for metal superhard carbon materials with excellent mechanical and electronic properties. However, despite theoretical predictions that carbon allotropes emerge in an endless stream, there are not many carbon materials that simultaneously exhibit metallic and superhard properties and enjoy favorable physical properties. Obviously, there is still a long way to go in designing and discovering breakthrough carbon materials with remarkable features. In this work, three superhard metal carbon materials are theoretically predicted and the results obtained show that these three carbon phases all have superhard metal characteristics and many advantageous properties, which are of great significance for enriching the gene pool of excellent materials and providing a solid theoretical basis for future experiments. More importantly, owing to their metallic

* **Corresponding author: Qingyang Fan,** College of Information and Control Engineering, Xi'an University of Architecture and Technology, Xi'an 710055, China; Shaanxi Key Laboratory of Nano Materials and Technology, Xi'an 710055, China, e-mail: qyfan_xidian@163.com, fanqy@xauat.edu.cn
* **Corresponding author: Qun Wei,** School of Physics and Optoelectronic Engineering, Xidian University, Xi'an 710071, China, e-mail: weiaqun@163.com
* **Corresponding author: Sining Yun,** Functional Materials Laboratory (FML), School of Materials Science and Engineering, Xi'an University of Architecture and Technology, Xi'an 710055, China, e-mail: alexsyun1974@aliyun.com, yunsining@xauat.edu.cn
Heng Liu, Li Jiang: College of Information and Control Engineering, Xi'an University of Architecture and Technology, Xi'an 710055, China
Wei Zhang, Yanxing Song: School of Microelectronics, Xidian University, Xi'an 710071, China
Xinhai Yu: Department of Mechanical and Electrical Engineering, Hetao College, Bayannur, Inner Mongolia 015000, China

and superhard properties, *o*P-C_{16}, *o*P-C_{20}, and *o*P-C_{24} may possess the opportunity to play applications in industrial and electronic fields.

In recent years, a considerable number of carbon allotropes and carbon-based materials have been identified. For instance, five carbon allotropes, *t*P12, *t*P16, *t*P24, *o*P12, and *o*P18, with nanotubes and cage types were proposed recently [2]. There are two-dimensional (2D) TPH-I carbon and TPH-II carbon obtained from pentagraphene through Stone-Wales conversion [3]. The electronic and mechanical properties of the new superhard indirect semiconductor *o*P8 carbon have also been predicted [4]. Li and Xing designed a superhard semiconductor material, *P2/m* C_{54}, which is a new type of semiconductor material that can be applied to frequency-hopping absorption filters [5]. TiO_2/graphite carbon nanocomposite materials, which can improve photocatalytic efficiency, are synthesized under certain temperatures and conditions [6]. In light of the synthesis of graphene with benzene as the precursor, a novel all-sp^2 hybridized 2D carbon allotrope with poly-butadiene–cyclooctatetraene framework is proposed [7]. By means of molecular dynamics simulation, the interface characteristics of carbon nanotube–polyimide nanocomposites have been systematically analyzed [8].

In particular, metallic carbon has attracted much attention due to its usefulness in electronic devices, superconductivity applications, and high-performance anode materials. By cross-linking graphene sheet with sp^3-hybridized carbon chains, Wang *et al.* established a new type of porous asymmetric carbon honeycomb (CHC), namely bco-C24 [9]. Using the self-assembled C8 skeleton of pentene as a building block, a series of 3D carbon allotropes (superpentalene-n family) were constructed [10]. A new type of orthogonal metal carbon phase *o*-C_{12} with high stability and hardness has been proposed, which is expected to be applied to actual electronic and mechanical equipment [11]. Zhang *et al.* proposed a metal superhard carbon allotrope C_{10}, which has an $sp^2 + sp^3$ hybrid carbon network in the orthorhombic unit cell and has a hardness of 58.70 GPa [12]. Liu *et al.* proposed two carbon polymorphs Orth-C10 and Orth-C10' with excellent superhard and conductive properties through first-principles calculations, which are more energetically stable than fullerene C60 at 0 GPa [13]. There are also paper carbon nanotubes that can replace aluminum foil as a current collector [14].

Recently, Wu *et al.* [15] reported a novel three-dimensional orthorhombic phase utilizing first-principles calculations. The novel three-dimensional orthorhombic phase, namely, C14-diamond, which was assembled with nanolayered sp^3 carbon in a diamond structure, was bonded with ethene-type –C═C– links and so C14-diamond is a superhard material and metallic carbon allotrope. In addition, the conductive direction of C14-diamond is also exhibited along these sp^2 carbon atoms. Additionally, Liu *et al.* [16] designed O-type and T-type carbon allotropes. The diamond nanostripes in O-type and T-type carbon allotropes are similar to C14-diamond and are also bonded with ethene-type –C═C– links. All the O-type and T-type carbon allotropes exhibited metallic properties, and the bulk modulus (B) and shear modulus (E) of O-type and T-type carbon allotropes exceeded 357 and 223 GPa, respectively.

In recent years, the focus of development has been to predict the properties of new materials and to design novel structures or some details in the new phases with function-oriented reverse design. However, compared with the huge demand in various fields such as modern industry, manufacturing, and aviation, carbon materials that are harder, more conductive, and lighter are still waiting for scientists to explore.

From ancient times to the present, carbon materials have been playing an increasingly important role in industrial applications, from initial heating materials to electronic materials and other functional materials. For example, supercapacitors based on carbon materials [17] have the same excellent characteristics as all-paper-based supercapacitor devices [18], such as fast charge and discharge speed, high power density, and long-term cycle stability. Complementary carbon nanotube transistors can even be used to build modern microprocessors [19]. Carbon nanomaterial-reinforced cement-based composites, which are stronger than traditional cement materials, smarter, and more durable, are also attracting attention [20]. Novel carbon materials and composite carbon materials [21] with excellent performance are closely related to modern engineering. The material gene bank is equivalent to the guiding light for the synthesis of new materials, so the theoretical importance of the exploration of new carbon structure is self-evident.

In this work, the three novel superhard metallic carbon allotropes (according to the number of carbon atoms in the conventional cell, denoted *o*P-C_{16}, *o*P-C_{20}, and *o*P-C_{24} below) are proposed in this work and these novel metallic carbon allotropes from the space group and graph theory (RG^2) code [22]. The crystal structures of *o*P-C_{16}, *o*P-C_{20}, and *o*P-C_{24} are similar to C14-diamond, O-type, and T-type carbon allotropes. The process is shown in graphical abstract. It can be seen that the structures of these three carbon allotropes are related and similar, and they are all composed of six-membered rings and ten-membered rings. From the ***ab*** plane, the

structure of *o*P-C_{16} is exactly identical to that of *o*P-C_{20}. The difference exists in ***bc*** and ***ac*** planes, as shown in the red wireframe in graphical abstract, that is the structure of *o*P-C_{20} possesses one more six-membered ring than that of *o*P-C_{16}. Interestingly, the addition of a six-membered ring to the structure of *o*P-C_{20} along the ***bc*** and ***ac*** planes converts it to the structure of *o*P-C_{24}. The hardness level of *o*P-C_{24} is higher than those of C14-diamond, O12 carbon, O20 carbon, T10 carbon, T18 carbon, and T26 carbon. Additionally, the conductive directions of *o*P-C_{16}, *o*P-C_{20}, and *o*P-C_{24} are also investigated in this work.

2 Computational method

The crystal structures of *o*P-C_{16}, *o*P-C_{20}, and *o*P-C_{24} are obtained from the random sampling strategy combining space group and graph theory (RG^2) [22]. For geometry optimization, ultrasoft pseudopotentials [23] are adopted in the interactions of the core electrons, and norm-conserving pseudopotentials [24] are employed for electronic band structure calculations. A generalized gradient approximation (GGA) proposed by Perdew *et al.* [25] and local density approximations (LDA), as developed by Ceperley and Alder and parameterized by Perdew and Zunger (CA-PZ) [26,27], is performed by utilizing the Cambridge Serial Total Energy Package [28] by means of density functional theory [29,30] calculations. The Broyden–Fletcher–Goldfarb–Shenno (BFGS) [31] minimization technique is used for geometry optimization. A plane wave basis set with an energy cut-off of 400 eV is used for *o*P-C_{16}, *o*P-C_{20}, and *o*P-C_{24}. A high-accuracy grid spacing of lower than $2\pi \times 0.025$/Å is selected utilizing the Monkhorst–Pack scheme [32] (for *o*P-C_{16}: $16 \times 15 \times 3$, *o*P-C_{20}: $16 \times 16 \times 2$, and *o*P-C_{20}: $16 \times 16 \times 2$).

For other carbon materials (C14-diamond [15], T10 carbon, T18 carbon, T26 carbon, O12 carbon, O20 carbon, O26 carbon [16], and C14 carbon [33]) for comparison, the cutoff energy of 400 eV is also used, and the *k*-points of the other carbon materials (T10 carbon: $16 \times 16 \times 4$, T18 carbon: $16 \times 16 \times 2$, T26 carbon: $16 \times 16 \times 2$, O12 carbon: $4 \times 16 \times 15$, O20 carbon: $2 \times 16 \times 16$, O26 carbon: $2 \times 16 \times 16$, C14-diamond: $2 \times 16 \times 16$, and C14 carbon: $16 \times 4 \times 11$) are also used for the high-accuracy grid spacing of lower than $2\pi \times 0.025$/Å. The Heyd–Scuseria–Ernzerhof (HSE06) hybrid functional [34] is adopted to estimate the electronic properties of *o*P-C_{16}, *o*P-C_{20}, and *o*P-C_{24}. The density functional perturbation theory [35] is employed to investigate the phonon spectra for *o*P-C_{16}, *o*P-C_{20}, and *o*P-C_{24}. First-principles calculations are favored by many researchers in the fields of condensed matter physics and computational materials science. Regarding the study of the physical properties of metallic carbon, some references [13,15,16,33] use first-principles calculations. Thus, in this work, first-principles calculations are adopted to study the physical properties of the three proposed carbon allotropes.

3 Results and discussion

The designed constructions of *o*P-C_{16}, *o*P-C_{20}, and *o*P-C_{24}, and their crystal structures are shown in graphical abstract. There are four sp^2 hybridization carbon atoms in all three structures, that is, there are two –C═C– bonds in the *o*P-C_{16}, *o*P-C_{20}, and *o*P-C_{24} crystal structures. The *o*P-C_{16}, *o*P-C_{20}, and *o*P-C_{24} carbon phases are established by the $sp^2 + sp^3$ hybrid bonding network in a three-dimensional formation. These three structures also contain different numbers of inequivalent atomic positions. *o*P-C_{16} has eight different inequivalent atomic positions, *o*P-C_{20} has ten different inequivalent atomic positions, and *o*P-C_{24} has twelve different inequivalent atomic positions. The optimal lattice parameters of *o*P-C_{16}, *o*P-C_{20}, and *o*P-C_{24} are presented in Table 1. Furthermore, the theoretical and experimental values of the lattice parameters for diamond are displayed in Table 1 for comparison. The estimated results obtained by using the GGA method are closer to the experimental values than those obtained by using LDA. Thus, all theoretical calculations in our article are performed at the GGA level.

The dynamic stability for *o*P-C_{16}, *o*P-C_{20}, and *o*P-C_{24} can be checked using phonon spectra. The phonon spectra of *o*P-C_{16}, *o*P-C_{20}, and *o*P-C_{24} are shown in Figure 1(a–c).

Table 1: Obtained lattice constants (Å), cell volume/atom *V* (Å^3), and density (g/cm^3) for *o*P-C_{16}, *o*P-C_{20}, *o*P-C_{24}, c-BN, and diamond

Materials	Method	*a*	*b*	*c*	*V*	*ρ*
*o*P-C_{16}	GGA	2.515	2.597	14.901	6.085	3.278
	LDA	2.488	2.563	14.742	5.877	3.394
*o*P-C_{20}	GGA	2.517	2.580	18.464	5.994	3.327
	LDA	2.489	2.547	18.265	5.791	3.444
*o*P-C_{24}	GGA	2.518	2.569	22.028	5.936	3.360
	LDA	2.490	2.537	21.789	5.736	3.477
c-BN	GGA	3.623			5.945	3.466
	LDA	3.577			5.721	3.602
	Exp.[a]	3.620			5.930	3.475
Diamond	GGA	3.566			5.668	3.519
	LDA	3.527			5.484	3.637
	Exp.[b]	3.567			5.673	3.516

[a]Ref. [41]; [b]Ref. [46].

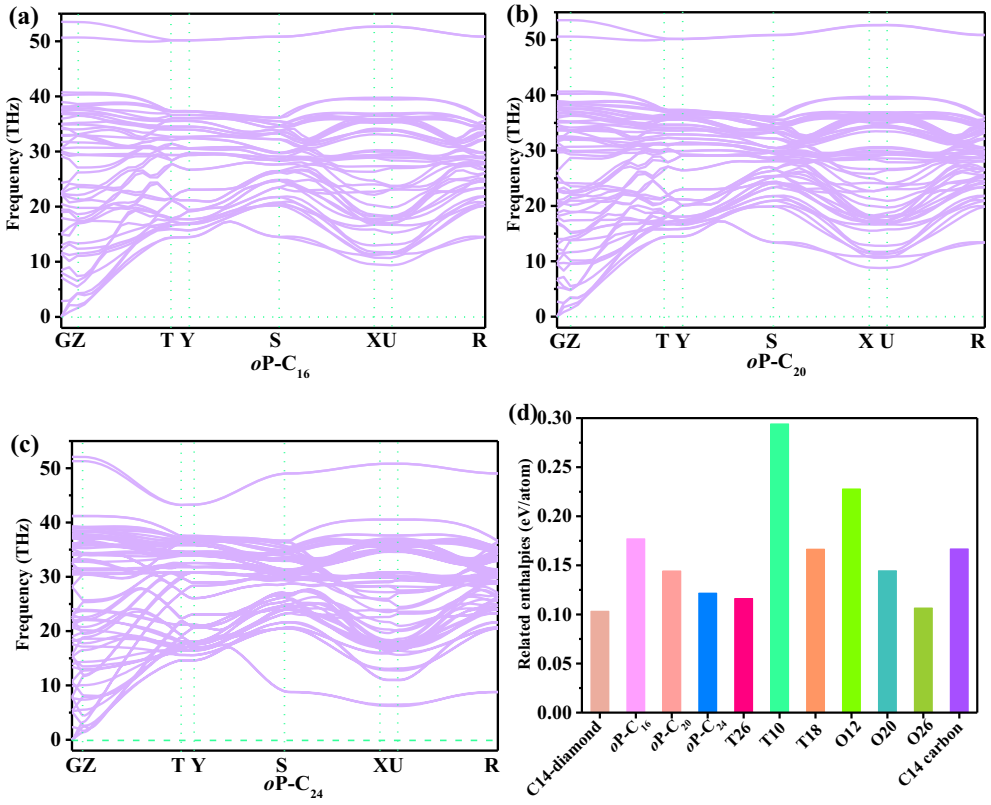

Figure 1: Phonon spectra of *o*P-C_{16} (a), *o*P-C_{20} (b), and *o*P-C_{24} (c), and the related enthalpies of other metallic carbon allotropes (d).

As described in ref. [15], the phonon modes greater than 40 THz chiefly originate from the vibration of sp^2 hybridization connected with the –C═C– bond, and the vibration frequency of sp^3 hybridization carbon atoms is mainly below 40 THz. In addition, most importantly, no hypothetical frequency is found in the whole Brillouin zone, demonstrating that the three predicted carbon allotropes are dynamically stable. Figure 1(d) shows the enthalpy per atom of *o*P-C_{16}, *o*P-C_{20}, and *o*P-C_{24}, including C14-diamond [15], T26 carbon, T10 carbon, T18 carbon, O18 carbon, O12 carbon, and O20 carbon [16] in the sp^2 + sp^3 bonding network and C14 carbon [33] in all sp^3 bonding networks compared with other carbon phases reported theoretically. As shown in Figure 1(d), *o*P-C_{24} is more stable than T10 carbon, T18 carbon, O12 carbon, O20 carbon, and C14 carbon in thermodynamics; *o*P-C_{20} is thermodynamically more stable than those of T10, O12, O20, and C14 carbon; and *o*P-C_{16} is thermodynamically more stable than those of T10 carbon and O12 carbon.

For the structure of a stable orthorhombic crystal system, the elastic constants C_{ij} should meet the mechanical elasticity criteria [36]: $C_{11} > 0$, $C_{11}C_{22} > C_{12}^2$, $C_{11}C_{22}C_{33} + 2C_{12}C_{13}C_{23} - C_{11}C_{23}^2 - C_{22}C_{13}^2 - C_{33}C_{12}^2 > 0$. Table 2 shows the estimated elastic parameters for *o*P-C_{16}, *o*P-C_{20}, and *o*P-C_{24}. All the acquired elastic parameters for *o*P-C_{16}, *o*P-C_{20}, and *o*P-C_{24} obey the above mechanical stability criteria. The C_{22} values of *o*P-C_{16}, *o*P-C_{20}, and *o*P-C_{24} are slightly lower than those of diamond, C14-diamond and C14 carbon, while they are higher than that of c-BN. Furthermore, the C_{11} and C_{33} of *o*P-C_{16}, *o*P-C_{20}, and *o*P-C_{24} are slightly higher than those of C14-diamond, C14 carbon, c-BN, and diamond. Nevertheless, the higher values of C_{11} and C_{33} indicate the greater horizontal and vertical linear compression resistance of the crystal [15]. The values of B and G are estimated by adopting Voigt-Reuss-Hill approximations according to the obtained elastic constants, and Young's modulus is estimated by $E = 9BG/(3B + G)$ based on the B and G values. The B_V, B_R, G_V and G_R are calculated as follows [37]: $B_V = (1/9)[C_{11} + C_{22} + C_{33} + 2(C_{12} + C_{13} + C_{23})]$, $G_V = (1/15)\ [C_{11} + C_{22} + C_{33} + 3(C_{44} + C_{55} + C_{66})(C_{12} + C_{13} + C_{23})]$, $B_R = \Delta[C_{11}(C_{22} + C_{33}\text{-}2C_{23}) + C_{22}(C_{33} - 2C_{13}) - 2C_{33}C_{12} + C_{12}(2C_{23} - C_{12}) + C_{13}(2C_{12} - C_{13}) + C_{23}(2C_{13} - C_{23})]^{-1}$, $G_R = 15\{4[C_{11}(C_{22} + C_{33} + C_{23}) + C_{22}(C_{33} + C_{13}) + C_{33}C_{12} - C_{12}(C_{23} + C_{12})C_{13}(C_{12} + C_{13})C_{23}(C_{13} + C_{23})]/A + 3[(1/C_{44}) + (1/C_{55}) + 1/C_{66}]\}^{-1}$, $A = C_{13}(C_{12}C_{23} - C_{13}C_{22}) + C_{23}(C_{12}C_{13} - C_{23}C_{11}) + C_{33}(C_{11}C_{22} - C_{12}^2)$. Although the B, G and E values for *o*P-C_{16}, *o*P-C_{20}, and *o*P-C_{24} are slightly lower than those

Table 2: The elastic constants (GPa), elastic modulus (GPa), and hardness (GPa) of metallic carbon allotropes, c-BN, and diamond

Materials	Method	C_{11}	C_{22}	C_{33}	C_{44}	C_{55}	C_{66}	C_{12}	C_{13}	C_{23}	B	G	E	H_{Chen}	$H_{M\text{-}O}$	$H_{L\text{-}O}$
*o*P-C_{16}	GGA	1,138	848	1,092	132	540	269	19	136	62	385	333	775	47.5	52.5	71.8
	LDA	1,206	912	1,151	103	568	273	20	156	76	414	325	773	41.4		
*o*P-C_{20}	GGA	1,141	908	1,087	136	545	307	20	131	73	395	347	805	49.6	55.6	69.3
	LDA	1,210	974	1,140	113	574	312	21	152	88	424	343	810	44.5		
*o*P-C_{24}	GGA	1,143	948	1,083	170	548	332	21	130	80	402	372	853	55.3	63.2	66.7
	LDA	1,212	1,014	1,139	155	578	339	22	150	96	431	377	876	52.0		
Diamond	GGA	1,053			563			120			431	522	1,116	94.3		
	LDA	1,104			598			140			461	549	1,179	95.3		
	Exp.[a]	1,076			577			125			442					

[a]Ref. [47].

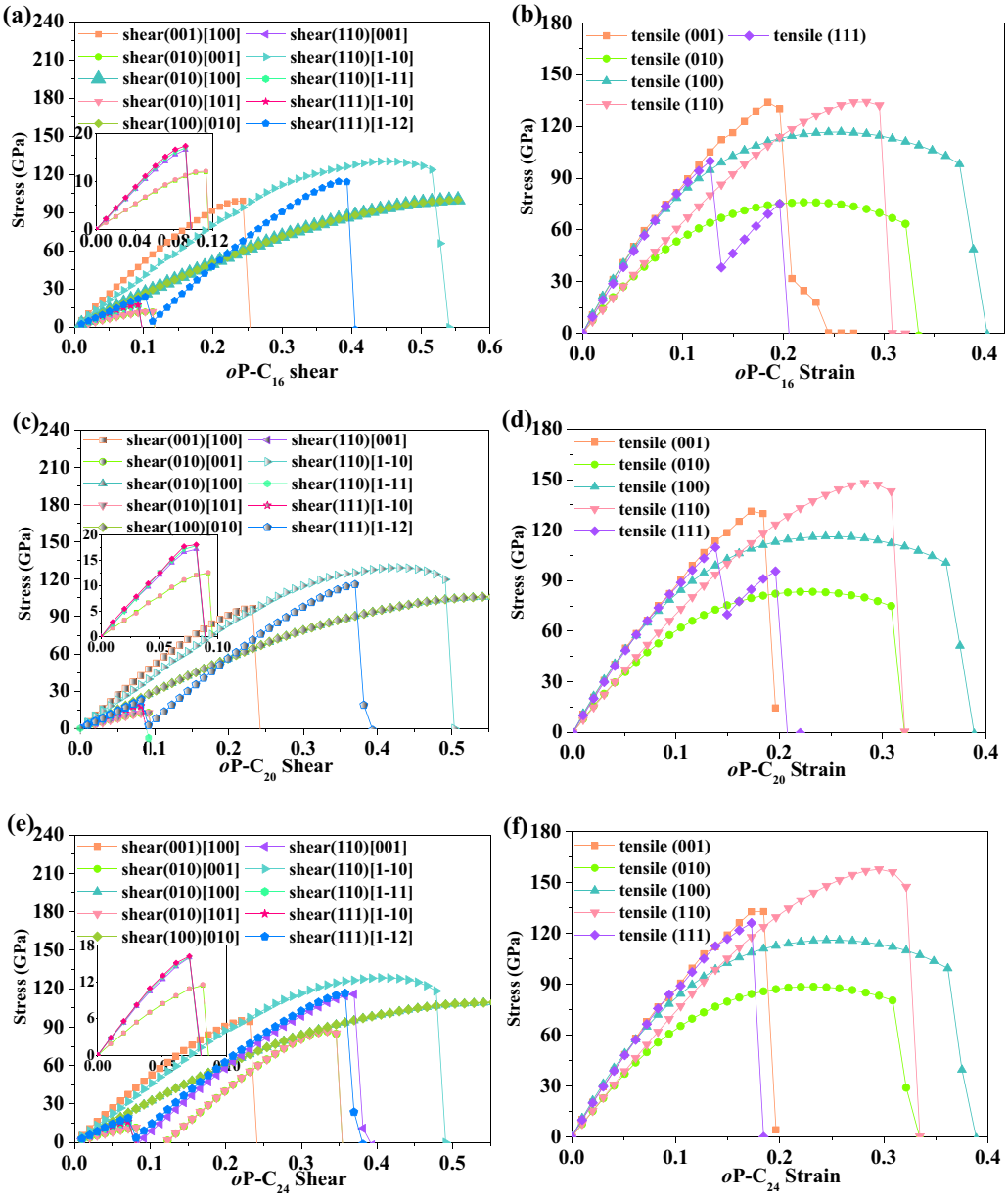

Figure 2: Calculated stress *vs* shear strain and the stress versus tensile strain for *o*P-C_{16} (a and b), *o*P-C_{20} (c and d), and *o*P-C_{24} (e and f) in principal symmetry directions.

Table 3: Obtained ideal shear strengths for *o*P-C_{16}, *o*P-C_{20}, and *o*P-C_{24} with the corresponding strains that produce the maximum stress (GPa)

	(001)[100]		(010)[001]		(010)[100]		(010)[101]		(100)[010]	
	Strain	**Stress**	**Strain**	**Stress**	**Strain**	**Stress**	**Strain**	**Stress**	**Strain**	**Stress**
*o*P-C_{16}	0.2431	99.2	0.1128	12.0	0.5537	100.2	0.1128	12.2	0.5537	100.2
*o*P-C_{20}	0.2319	96.6	0.0918	12.5	0.5410	105.9	0.0918	12.6	0.5537	105.9
*o*P-C_{24}	0.2319	94.4	0.0814	11.5	0.5537	109.4	0.0814	11.6	0.5537	109.4
	(110)[001]		**(110)[1–10]**		**(110)[1–11]**		**(111)[1–10]**		**(111)[1–12]**	
	Strain	**Stress**	**Strain**	**Stress**	**Strain**	**Stress**	**Strain**	**Stress**	**Strain**	**Stress**
*o*P-C_{16}	0.0918	16.6	0.4538	130.3	0.0918	17.0	0.0918	17.5	0.3815	114.4
*o*P-C_{20}	0.0814	17.2	0.4294	129.3	0.0814	17.9	0.0814	18.1	0.3696	115.8
*o*P-C_{24}	0.0711	16.2	0.4053	128.5	0.0711	16.1	0.0711	16.2	0.3578	116.5

Table 4: Calculated ideal tensile strengths for *o*P-C_{16}, *o*P-C_{20}, *o*P-C_{24} with the corresponding strains that produce the maximum stress (GPa)

	[001]		[010]		[100]		[110]		[111]	
	Strain	**Stress**	**Strain**	**Stress**	**Strain**	**Stress**	**Strain**	**Stress**	**Strain**	**Stress**
*o*P-C_{16}	0.1843	134.2	0.2202	75.9	0.2572	116.6	0.2824	134.4	0.1268	99.8
*o*P-C_{20}	0.1726	131.4	0.2202	83.4	0.2447	116.3	0.2821	148.1	0.1381	109.8
*o*P-C_{24}	0.1726	132.7	0.2324	88.6	0.2447	116.1	0.2953	157.9	0.1726	126.2

of C14-diamond, C14 carbon, and diamond, they are higher than those of O12 carbon and T10 carbon, while the bulk moduli of *o*P-C_{16}, *o*P-C_{20}, and *o*P-C_{24} are greater than that of c-BN.

Using Chen's model [38] to estimate hardness, the related results of their carbon materials within the GGA level are also shown in Table 2. From Table 2, the hardness values of *o*P-C_{16}, *o*P-C_{20}, and *o*P-C_{24} are estimated to be 47.5, 49.6, and 55.3 GPa, respectively. The hardness value of C14-diamond determined in the same way is 53.1 GPa, which is close to the previously reported hardness value (55.8 GPa [15]). In this work, the hardness values of *o*P-C_{16}, *o*P-C_{20}, and *o*P-C_{24} are greater than those of O12 carbon (39.9 GPa), T10 carbon (25.6 GPa), T18 carbon (34.8 GPa), and T26 carbon (43.8 GPa). Furthermore, the hardness value of *o*P-C_{20} is also higher than that of O20 carbon (48.8 GPa), and the hardness value of *o*P-C_{24} is also higher than those of C14-diamond and O28 carbon (54.3 GPa). In order to verify the superhardness of the three proposed carbon allotropes, $H_{M\text{-}O}$ [39] and $H_{L\text{-}O}$ model [40] are employed. Here, $H_{M\text{-}O}$ can be obtained based on Poisson's ratio and Young's modulus using the following equation [39]: $H_{M\text{-}O} = 0.096\,E\,(1–8.5\nu + 19.5\nu^2)(1–7.5\nu + 12.2\nu^2 + 19.6\nu^3)^{-1}$. The calculated hardness levels of *o*P-C_{16}, *o*P-C_{20}, and *o*P-C_{24} are 52–64 and 66–72 GPa, respectively, which are all greater than 40 GPa. All these three methods prove the fact that *o*P-C_{16}, *o*P-C_{20}, and *o*P-C_{24} have superhard characteristics.

To have a better understanding of the potential application of these carbons structures with superhard and metal properties, the stress–strain curves of the three carbon phases proposed by us under the tensile and shear strains in the low-index directions are calculated. The shear strength and tensile strength of *o*P-C_{16}, *o*P-C_{20}, and *o*P-C_{24} as functions of shear strain and tensile strain within the GGA functional are plotted in Figure 2. The turning point on the stress–strain curve indicates the ideal tensile strength or the ideal shear strength. The ideal shear strengths along the different shear directions of *o*P-C_{16}/*o*P-C_{20}/*o*P-C_{24} are listed in Table 3. For *o*P-C_{16}/*o*P-C_{20}/*o*P-C_{24}, the peak shear stresses are 12.0/12.5/11.5, 12.2/12.6/11.6, 16.6/17.2/16.2, 17.0/17.9/16.1, and 17.5/18.1/16.2 GPa along the (010)[001], (010)[101], (110)[001], (110)[1–11], and (111)[1–10] directions, respectively. The possible cause is also the fracture of sp^2 –C═C– bonds, similar to C14-diamond, O12 carbon, O20 carbon, O28 carbon, T10 carbon, T18 carbon, and T26 carbon. As discussed in Reference [16], although the three proposed carbon allotropes in this work are metals, their ideal shear strengths are also greater than those of common

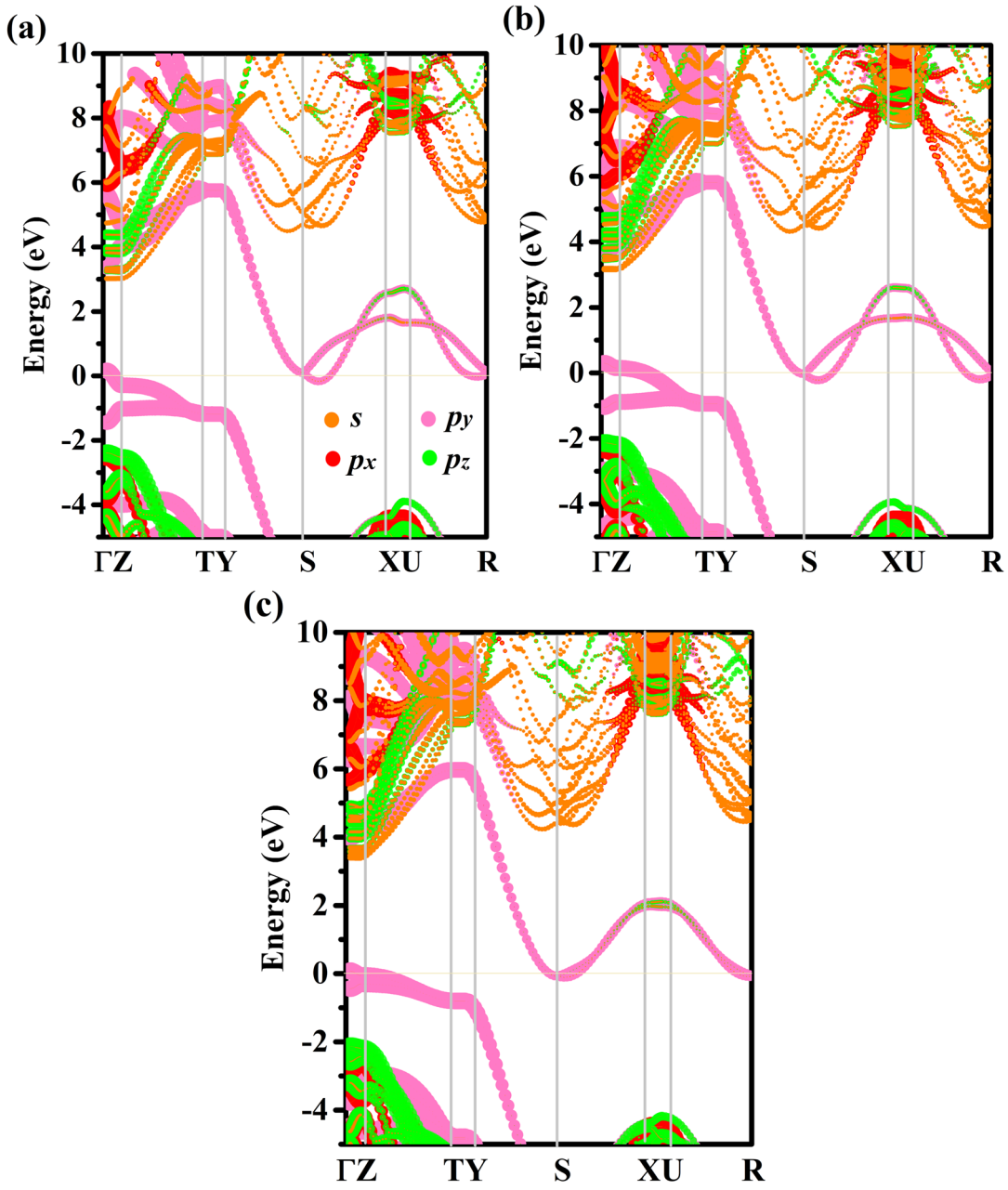

Figure 3: Band structures of *o*P-C_{16} (a), *o*P-C_{20} (b), and *o*P-C_{24} (c).

metals such as Cu (4.0 GPa) [41], Al (3.4 GPa) [41], and Fe (6.40 GPa) [42]. In addition, the three kinds of carbon allotropes proposed by us can only break when the shear strain along these directions is above 0.07, while T18 carbon and T26 carbon break when the shear strain is 0.06 and 0.04, respectively. The minimum peak shear stresses along the (001)[100], (010)[100], (100)[010], (110)[1–10], and (111) [1–12] directions of *o*P-C_{16}/*o*P-C_{20}/*o*P-C_{24} are 94.4 GPa, which is slightly larger than that of O28 carbon along the (100)[010] direction.

The tensile strengths of *o*P-C_{16}, *o*P-C_{20}, and *o*P-C_{24} as functions of tensile strain within the GGA functional are displayed in Figure 2(b), (d), and (e), respectively. The ideal tensile strengths along the different tensile directions of *o*P-C_{16}/*o*P-C_{20}/*o*P-C_{24} are presented in Table 4. From Figure 2(b), (d), and (e), it can be seen that the tensile stress–strain curve of *o*P-C_{16}/*o*P-C_{20}/*o*P-C_{24} shows a plastic deformation relationship along the [010] and [100] directions, a relationship similar to that of O20 carbon. For the [001], [100], [110], and [111] directions, the ideal tensile

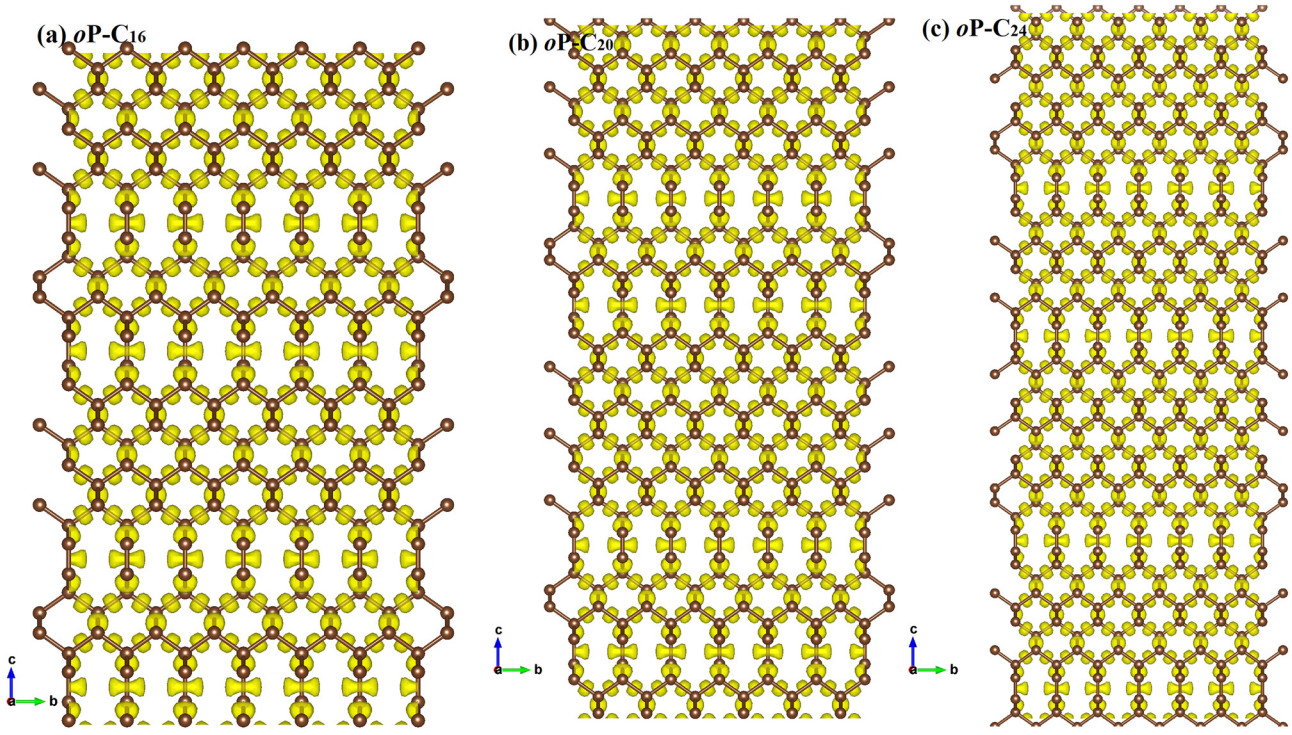

Figure 4: The electron localization function (ELF) of oP-C_{16} (a), oP-C_{20} (b), and oP-C_{24} (c) with an isosurface level set to 0.75.

strength is basically greater than 100 GPa, and the maximum is 157.9 GPa, which is the [110] direction of oP-C_{24}. Although for the [010] direction, the ideal tension strengths of oP-C_{16}, oP-C_{20}, and oP-C_{24} are the worst, reaching 75.9, 83.4, and 88.6 GPa, respectively. For the [111] direction, the ideal tensile strengths of oP-C_{16}, oP-C_{20}, and oP-C_{24} are 99.8, 109.8, and 126.2 GPa, respectively. The smallest ideal tension strength of the three carbon materials along the [111] direction is nearly 18 GPa greater than that of diamond, 30 GPa greater than that of O28 carbon, and 60 GPa larger than that of T10 carbon. The high values of B modulus, hardness, and ideal strength provide these new materials broad application prospects in wear-resistant metal coatings and cutting tools.

To analyze the electronic band structures of oP-C_{16}, oP-C_{20}, and oP-C_{24}, the projected weights of each kind of orbital of oP-C_{16}, oP-C_{20}, and oP-C_{24} using the Heyd–Scuseria–Ernzerhof (HSE06) hybrid functional are plotted in Figure 3. By showing the weights of the electrons in different orbits, it is found that the conduction band minimum between the S and X points and the valence band maximum at the Γ point both cross the Fermi surface. Similar to T10 carbon, T18 carbon, T26 carbon, O12 carbon, O20 carbon, O20 carbon, and C14-diamond, oP-C_{16}, oP-C_{20}, and oP-C_{24} all have metallic properties. In addition, the Fermi level is chiefly provided by the p_y electrons. In the Brillouin zone, the coordinates for oP-C_{16}, oP-C_{20}, and oP-C_{24} are taken Γ (0.0, 0.0, 0.0), Z (0.0, 0.0, 0.5), T (−0.5, 0.0, 0.5), Y (−0.5, 0.0, 0.0), S (−0.5, 0.5, 0.0), X (0.0, 0.5, 0.0), U (0.0, 0.5, 0.5), and R (−0.5, 0.5, 0.5) of the high symmetry points. To visualize the chemical bonding in oP-C_{16}, oP-C_{20}, and oP-C_{24}, the electron localization function (ELF) [43,44] using an isosurface value of 0.75 is demonstrated in Figure 4(a–c). The calculated ELF of oP-C_{16}, oP-C_{20}, and oP-C_{24} further indicates the strong covalent C–C bonding feature; at the same time, it can be clearly seen that the σ bond is formed by the sp^2 hybrid carbon atom. To further analyze in which direction the three metal carbon materials conduct electricity, the charge density of the band decomposition observed along the a-axis and b-axis of oP-C_{16}, oP-C_{20}, and oP-C_{24} are shown in Figure 5(a–f), which suggests that the conductive directions of oP-C_{16}, oP-C_{20}, and oP-C_{24} are all exhibited along the a- and b-axis.

To achieve additional information for probable future experimental examination, the simulation of x-ray diffraction (XRD) patterns for oP-C_{16}, oP-C_{20}, and oP-C_{24} along with that of diamond are shown in Figure 6. Diamond possesses two diffraction peaks, which appear at 43.93 and 75.29° of (111) and (220), respectively, and in the present work, they are in good agreement with the experimental XRD spectra of 43.9 and 75.2° for (111) and (220) of diamond [45], indicating that the performed simulation method is reliable. Because of the same space

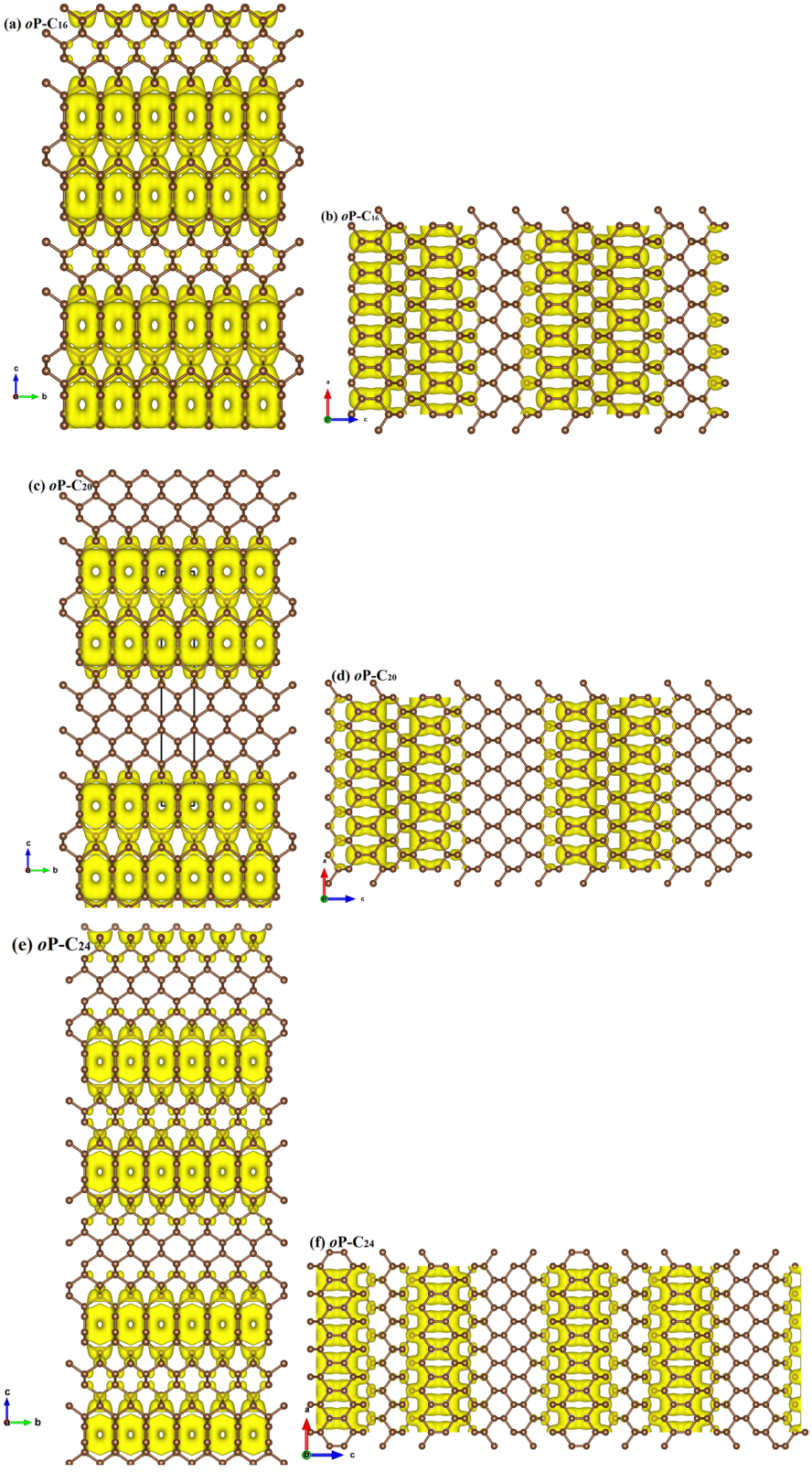

Figure 5: The calculated band decomposed charge density in the energy range of $E_F - 1 \sim E_F + 1$ eV for *o*P-C_{16} (a and b), *o*P-C_{20} (c and d), and *o*P-C_{24} (e and f) along the *a* and *b* axes with an isovalue level set to 0.005.

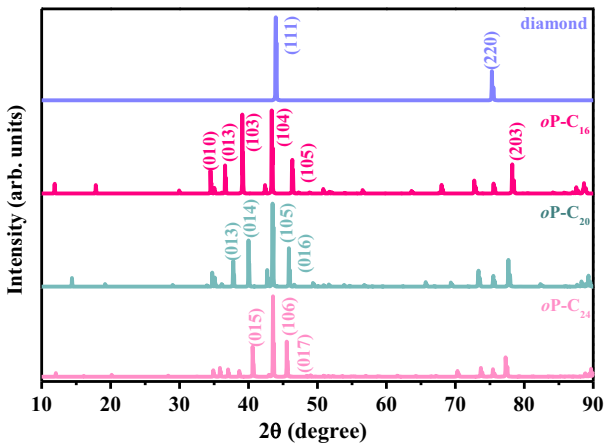

Figure 6: Simulated XRD patterns of *o*P-C_{16}, *o*P-C_{20}, *o*P-C_{24}, and diamond, using an x-ray wavelength (1.5406 Å) with a copper source for simulation in this work.

groups of *o*P-C_{16}, *o*P-C_{20}, and *o*P-C_{24}, their XRD spectra are also very close, which is reflected in the fact that all their three strong peaks appear between 35° and 48°. The peak intensities in the XRD patterns of *o*P-C_{16}, *o*P-C_{20}, and *o*P-C_{24} are not equivalent. The strongest peaks are (104), (105), and (106), which are located around 43.97, 43.48, and 43.55° for *o*P-C_{16}, *o*P-C_{20}, and *o*P-C_{24}, respectively. For *o*P-C_{16} and *o*P-C_{20}, their stronger peaks both contain the two peaks (013) and (105), while the stronger peaks of *o*P-C_{24} are (015), (106), and (017). Apart from these major diffraction peaks, several other weak diffraction peaks appeared in the XRD spectrum, such as, for (101) peaks, the diffraction angles are 36.19, 35.99, and 35.87° for *o*P-C_{16}, *o*P-C_{20}, and *o*P-C_{24}, respectively; for (111) peaks, the diffraction angles are 50.86, 50.89, and 50.91° for *o*P-C_{16}, *o*P-C_{20}, and *o*P-C_{24}, respectively. These XRD features have important significance and guidance for identifying the structures of *o*P-C_{16}, *o*P-C_{20}, and *o*P-C_{24} in future experiments.

4 Conclusion

In summary, three new carbon allotropes, *o*P-C_{16}, *o*P-C_{20}, and *o*P-C_{24}, with metallic and superhard properties are proposed theoretically through first-principles calculations. These three new types of carbon structures possess many outstanding characteristics. *o*P-C_{16} is energetically more favorable than T10 and O12 carbon, while *o*P-C_{20} and *o*P-C_{24} are more favorable in energy than T18, O12, and O20 carbon. More importantly, *o*P-C_{16}, *o*P-C_{20}, and *o*P-C_{24} enjoy hardness levels of 47.5, 49.6, and 55.3 GPa, respectively. For *o*P-C_{16}/*o*P-C_{20}/*o*P-C_{24}, the peak shear stresses are 11.5–18.1 GPa along the (010)[001], (010)[101], (110)[001], (110)[1–11], and (111)[1–10] directions, respectively. Although the three carbon allotropes proposed in this work are metals, their ideal shear strengths are also greater than those of common metals such as Cu, Fe, and Al. The p_y electrons cross the Fermi level, revealing that *o*P-C_{16}, *o*P-C_{20}, and *o*P-C_{24} exhibit metallicity. Superhard, conductive, and other excellent physical properties make *o*P-C_{16}, *o*P-C_{20}, and *o*P-C_{24} have great application potential in multifunctional devices under extreme conditions, and they are also potential materials for electronic devices and mechanical tools. The theoretical research in this article is of great significance for enriching the gene pool of excellent materials and providing a solid theoretical basis for future experiments.

Funding information: This work was supported by the National Natural Science Foundation of China (Nos. 61804120, 61803294, and 61901162); the China Postdoctoral Science Foundation (Nos. 2019TQ0243 and 2019M663646); key scientific research plan of Education Department of Shaanxi Provincial Government (Key Laboratory Project) (No. 20JS066); the Young Talent fund of University Association for Science and Technology in Shaanxi, China (No. 20190110); and the National Key R&D Program of China (No. 2018YFB1502902); and Key Program for International S&T Cooperation Projects of Shaanxi Province (No. 2019KWZ-03).

Author contributions: All authors have accepted responsibility for the entire content of this manuscript and approved its submission.

Conflict of interest: The authors state no conflict of interest.

References

[1] Takeo O. Crystal structures of perovskite halide compounds used for solar cells. Rev Adv Mater Sci. 2020;59(1):264–305.
[2] Fan Q, Wang H, Song Y, Zhang W, Yun S. Five carbon allotropes from Squaroglitter structures. Comput Mater Sci. 2020;178:109634.
[3] Zhang W, Chai C, Fan Q, Song Y, Yang Y. Two-dimensional carbon allotropes with tunable direct band gaps and high carrier mobility. Appl Surf Sci. 2021;537:147885.
[4] Fan Q, Li C, Yang R, Yu X, Zhang W, Yun S. Stability, mechanical, anisotropic and electronic properties of oP8 carbon: a superhard carbon allotrope in orthorhombic phase. J Solid State Chem. 2021;294:121894.

[5] Li XZ, Xing MJ. Prediction of a novel carbon allotrope from first-principle calculations: a potential superhard material in monoclinic symmetry. Mater Chem Phys. 2020;242:122480.
[6] Janusz T, Niko G, Grzegorz Z, Malwina P, Aleksander G, Ewelina KN, et al. Magnetic properties of TiO2/graphitic carbon nanocomposites. Rev Adv Mater Sci. 2019;58(1):107–22.
[7] Zhang W, Chai C, Fan Q, Song Y, Yang Y. PBCF-graphene: a 2D Sp^2 hybridized honeycomb carbon allotrope with a direct band gap. ChemNanoMat. 2020;6:139–47.
[8] Jiang Q, Tallury SS, Qiu Y, Pasquinelli MA. Interfacial characteristics of a carbon nanotube-polyimide nanocomposite by molecular dynamics simulation. Nanotechnol Rev. 2020;9(1):136–45.
[9] Wang S, Yang B, Ruckenstein E, Chen H. Bco-C_{24}: a new 3D Dirac nodal line semi-metallic carbon honeycomb for high performance metal-ion battery anodes. Carbon. 2020;159:542–8.
[10] Zhang W, Chai C, Fan Q, Song Y, Yang Y. Metallic and semiconducting carbon allotropes comprising of pentalene skeletons. Diam Relat Mater. 2020;109:108063.
[11] Zhou Y, Liu Z, Gan LH. o-C_{12}: a novel orthorhombic metallic superhard carbon phase. Solid State Sci. 2021;119:106607.
[12] Zhang W, Chai C, Fan Q, Song Y, Yang Y. Superhard three-dimensional carbon with one-dimensional conducting channels. New J Chem. 2020;44(45):19789–95.
[13] Liu L, Hu M, Zhao Z, Pan Y, Dong H. Superhard conductive orthorhombic carbon polymorphs. Carbon. 2020;158:546–52.
[14] Ventrapragada LK, Creager SE, Rao AM, Podila R. Carbon nanotubes coated paper as current collectors for secondary Li-ion batteries. Nanotechnol Rev. 2019;8(1):18–23.
[15] Wu X, Shi X, Yao M, Liu S, Yang X, Zhu L, et al. Superhard three-dimensional carbon with metallic conductivity. Carbon. 2017;123:311–7.
[16] Liu Y, Jiang X, Fu J, Zhao J. New metallic carbon: Three dimensionally carbon allotropes comprising ultrathin diamond nanostripes. Carbon. 2018;126:601–10.
[17] Jiang Q, Tallury SS, Qiu Y, Pasquinelli MA. Recent development of supercapacitor electrode based on carbon materials. Nanotechnol Rev. 2019;8(1):35–49.
[18] Xiong C, Li M, Han Q, Zhao W, Dai L, Ni Y. Screen printing fabricating patterned and customized full paper-based energy storage devices with excellent photothermal, self-healing, high energy density and good electromagnetic shielding performances. J Mater Sci Technol. 2022;97:190–200.
[19] Hills G, Lau C, Wright A, Fuller S, Bishop MD, Srimani T, et al. Modern microprocessor built from complementary carbon nanotube transistors. Nature. 2019;572(7771):595–602.
[20] Du M, Jing H, Gao Y, Su H, Fang H. Carbon nanomaterials enhanced cement-based composites: advances and challenges. Nanotechnol Rev. 2020;9(1):115–35.
[21] Xiong C, Li B, Duan C, Dai L, Nie S, Qin C, et al. Supercapacitor, strain sensing and moisture-electric generation applications. Chem Eng J. 2021;418:129518.
[22] Shi X, He C, Pickard CJ, Tang C, Zhong J. Stochastic generation of complex crystal structures combining group and graph theory with application to carbon. Phys Rev B. 2018;97(1):014104.
[23] Vanderbilt D. Soft self-consistent pseudopotentials in a generalized eigenvalue formalism. Phys Rev B. 1990;41(11):7892–5.
[24] Hamann DR, Schluter M, Chiang C. Norm-conserving pseudopotentials. Phys Rev Lett. 1979;43(20):1494–7.
[25] Perdew JP, Burke K, Ernzerhof M. Generalized gradient approximation made simple. Phys Rev Lett. 1996;78(7):1396.
[26] Ceperley DM, Alder BJ. Ground state of the electron gas by a stochastic method. Phys Rev Lett. 1980;45(7):566.
[27] Perdew JP, Zunger A. Self-interaction correction to density-functional approximations for many-electron systems. Phys Rev B. 1981;23(10):5048–79.
[28] Clark SJ, Segall MD, Pickard CJ, Hasnip PJ, Probert MIJ, Refson K, et al. First principles methods using CASTEP. Z Kristallogr. 2005;220:567–70.
[29] Hohenberg P, Kohn W. Inhomogeneous electron gas. Phys Rev. 1964;136(3):B864.
[30] Kohn W, Sham LJ. Self-consistent equations including exchange and correlation effects. Phys Rev. 1965;140(4A):A1133.
[31] Pfrommer BG, Côté M, Louie SG, Cohen ML. Relaxation of crystals with the quasi-Newton method. J Comput Phys. 1997;131(1):233–40.
[32] Monkhorst HJ, Pack JD. Special points for Brillouin-zone integrations. Phys Rev B. 1976;13(12):5188.
[33] Yang X, Lv C, Liu S, Zang J, Qin J, Du M, et al. Orthorhombic C14 carbon: a novel superhard sp3 carbon allotrope. Carbon. 2020;156:309–12.
[34] Heyd J, Scuseria GE, Ernzerhof M. Hybrid functionals based on a screened coulomb potential. J Chem Phys. 2003;118(18):8207–15.
[35] Baroni S, de Gironcoli S, dal Corso A, Giannozzi P. Phonons and related crystal properties from density-functional perturbation theory. Rev Mod Phys. 2001;73(2):515.
[36] Mouhat F, Coudert FX. Necessary and sufficient elastic stability conditions in various crystal systems. Phys Rev B. 2014;90(22):224104.
[37] Wu ZJ, Zhao EJ, Xiang HP, Hao XF, Liu XJ, Meng J. Crystal structures and elastic properties of superhard IrN_2 and IrN_3 from first principles. Phys Rev B. 2007;76(5):054115.
[38] Chen XQ, Niu H, Li D, Li Y. Modeling hardness of polycrystalline materials and bulk metallic glasses. Intermetallics. 2011;19(9):1275–81.
[39] Mazhnik E, Oganov AR. A model of hardness and fracture toughness of solids. J Appl Phys. 2019;126(12):125109.
[40] Lyakhov AO, Oganov AR. Evolutionary search for superhard materials: methodology and applications to forms of carbon and TiO2. Phys Rev B. 2019;84(9):92103.
[41] Roundy D, Krenn CR, Cohen ML, Morris JW. Ideal shear strengths of fcc aluminum and copper. Phys Rev Lett. 1999;82(13):2713–6.
[42] Krenn CR, Roundy D, Morris JW, Cohen ML. Ideal strengths of bcc metals. Mater Sci Eng A. 2001;319:111–4.
[43] Silvi B, Savin A. Classification of chemical bonds based on topological analysis of electron localization functions. Nature. 1994;371(6499):683–6.
[44] Becke AD, Edgecombe KE. A simple measure of electron localization in atomic and molecular systems. J Chem Phys. 1990;92:5397–403.
[45] Mao WL, Mao HK, Eng P, Trainor T. Bonding changes in compressed superhard graphite. Science. 2003;302(5644):425–7.
[46] Petrescu ML. Boron nitride theoretical hardness compared to carbon polymorphs. Diam Relat Mater. 2004;13(10):1848–53.
[47] Grimsditch M, Zouboulis ES, Polian A. Elastic constants of boron nitride. J Appl Phys. 1994;76:832.